Journal of The Electrochemical Society, **149** (8) G461-G473 (2002)
0013-4651/2002/149(8)/G461/13/$7.00 © The Electrochemical Society, Inc.

Transient Adsorption and Desorption in Micrometer Scale Features

Matthias K. Gobbert,[a,*,z] Samuel G. Webster,[a] and Timothy S. Cale[b,*]

[a]*Department of Mathematics and Statistics, University of Maryland, Baltimore County, Baltimore, Maryland 21250, USA*
[b]*Focus Center-New York, Rensselaer: Interconnections for Gigascale Integration, Rensselaer Polytechnic Institute, Troy, New York 12180-3590, USA*

We present a Boltzmann equation-based model for transport and reaction in micrometer-scale features such as those found in integrated circuit fabrication. We focus on the adsorption and desorption of one species to understand the transient responses to step changes at the reactor scale. The transport model has no adjustable parameters; the assumptions are detailed. Adsorption and desorption reactions and rates are written as simple reversible Langmuir rate expressions. Kinetic parameter values are chosen for demonstration. Results for the transient behavior of number density, flux to the surface, and the surface coverage are related to those that might occur during the adsorption and purge steps in an atomic layer deposition process. We conclude that for reasonable surface kinetics, the time scale for transport is much shorter than the time scale for adsorption and desorption and that an analytical model provides reasonable estimates for processing times.
© 2002 The Electrochemical Society. [DOI: 10.1149/1.1486452] All rights reserved.

Manuscript submitted August 3, 2001; revised manuscript received February 12, 2002. Available electronically June 17, 2002.

In an ideal atomic layer deposition (ALD) process, the deposition of solid material on the substrate is accomplished one atomic or molecular layer at a time, in a self-limiting fashion; this property is responsible for the recent interest in ALD. To accomplish this, a representative ALD process consists of repeating a sequence of reactant flows and reactor purges. In the first step of a cycle, a gaseous species (A) is directed into the reactor, and (ideally) one monolayer adsorbs onto the surface. After purging the reactor, a second gaseous reactant (B) is directed through the reactor. A self-limiting chemical reaction forms the next layer of deposited film. By repeating this cycle of reactant flows and purges, a film of ideally uniform and controlled thickness is deposited.[1-4]

Although ALD has the potential to deposit films of uniform thickness, to keep average rates at reasonably high levels, high switching frequencies of reactants and purges are desired. A pulse frequency that is too high may lead to nonuniform film deposition on the feature scale, on the wafer scale, or both. As a start toward understanding species transport in features during ALD, we model the adsorption of species A and the desorption that occurs during the following purge in one cycle of a ALD process. We use a Boltzmann equation-based transport model with no adjustable parameters. The chemical reaction model used for the adsorption and desorption rates are those found in typical mechanistic representations of simple reversible Langmuir adsorption.

We consider the case in which the flux of reactive species from the source volume to the wafer surface is constant with time, either at zero or at some selected value. Essentially, we idealize the transients at the reactor scale, and focus on modeling feature scale processes in response to these idealized steps in concentration above the wafer surface. More general boundary conditions at the interface between the wafer surface and the reactor volume are possible, but the results presented below provide considerable insight. We also assume that the process is isothermal in time and space.

For an introduction to a deterministic approach to feature scale transport and reaction modeling and simulation that has been used for deposition and etch processes, see Ref. 5, 6. That approach is valid for processes for which a pseudo-steady assumption holds; *i.e.*, for which changes on the feature scale are slow relative to the redistribution of fluxes in the feature. On the other hand, transients are central to ALD, and we need to start with a transient model. In this paper, we consider cases for which the fluxes to the wafer surface are constant with time (with the exception of step changes). For transients that are present on the time scale of processes, see a discussion on programmed rate processing in Ref. 7. For a discussion on the dimensionality of transport modeling relative to the dimensionality of surface representation, see Ref. 8.

We describe the model in the next section, then outline the numerical approach in the following section. We then present and discuss some simulation results for the adsorption and purge steps of an ALD process. Preliminary results for adsorption without considering desorption and with different choices of reference quantities and with a less precise estimate for the equilibrium fluxes have been presented.[9]

The Model

The domain.—The domain, Ω, of the feature scale model includes the interior area of one feature and a small part of the gas domain above and around the feature mouth; a schematic of a two-dimensional (2-D) domain chosen as a cross section of a typical feature is shown in Fig. 1a. The differential equation needs to be accompanied by boundary conditions along $\partial\Omega$, which is comprised of three parts with different boundary conditions: $\partial\Omega = \Gamma_w \cup \Gamma_t \cup \Gamma_s$. Here, Γ_w denotes the portion of the boundary along the solid wafer surface, Γ_t is the top of the domain that forms the interface to the bulk of the reactor, and Γ_s denotes the union of the portions of the boundary on the sides of the domain.

The differential equations in the gaseous domain.—The flow of a rarefied gas is described by the Boltzmann equation[10-12] for each gaseous species

$$\frac{\partial f^{(i)}}{\partial t} + v\nabla_x f^{(i)} = \sum_{j=0}^{1} Q_{ij}(f^{(i)}, f^{(j)}) \qquad i = 0,\ 1 \qquad [1]$$

The unknown variables are the density distribution functions $f^{(i)}(x,v,t)$, *i.e.*, the number of molecules of species i at position $x = (x_1,x_2,x_3) \in \Omega \subset \mathbb{R}^3$ with velocity $v = (v_1, v_2, v_3) \in \mathbb{R}^3$ at time $t \geq 0$. The $f^{(i)}$ have to be determined for all points x in the domain $\Omega \subset \mathbb{R}^3$ and for all possible velocities $v \in \mathbb{R}^3$. The distribution functions are scaled such that

$$c_i(x,t) := \int_{\mathbb{R}^3} f^{(i)}(x,v,t)\,dv \qquad i = 0,\ 1 \qquad [2]$$

gives the molar concentration of species i at $x \in \Omega$ at time t. As written, Eq. 1 is appropriate for ALD with one inert background species I with index $i = 0$ and reactive species A with $i = 1$. The left side describes the transport of species i. The right side describes

* Electrochemical Society Active Member.
z E-mail: gobbert@math.umbc.edu

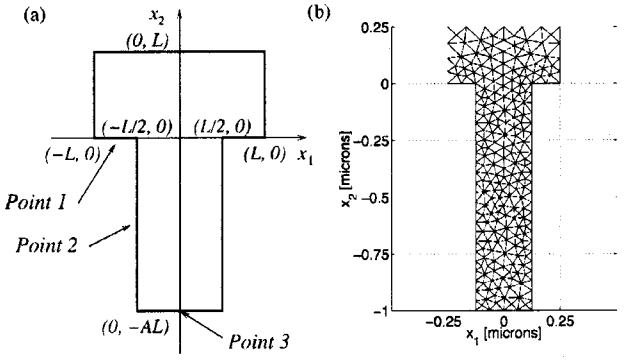

Figure 1. (a) Schematic of a two-dimensional domain defining length L and aspect ratio A. (b) Numerical mesh for the feature with $L = 0.25$ μm and aspect ratio $A = 4$.

the effect of collisions among molecules of all species, in which the collision operators Q_{ij} model the collisions between molecules of species i and j. The following paragraphs show how we treat collisional transport of reactive species in a background gas. This derivation is important to arrive at the appropriate dimensionless formulation of the Boltzmann equation for free molecular flow.

Assuming that the reactive species $j = 1$ is an order of magnitude less concentrated than the background gas 0, it can be shown that it is justified to keep only the collision operators Q_{i0} and neglect Q_{i1} in every equation $i = 0, 1$. If we also assume that the background gas is uniformly distributed in space ($\nabla_x f^{(0)} = 0$), at equilibrium ($\partial f^{(0)}/\partial t = 0$), and inert (does not react with the species $j = 1$), then the equation for $f^{(0)}$ is decoupled from the remaining one for the reactive species and consists in fact of $Q_{00}(f^{(0)}, f^{(0)}) = 0$ only, which has as a solution a Maxwellian[10,11]

$$f^{(0)}(x,v,t) = M_0^{\text{ref}}(v) := \frac{c_0^{\text{ref}}}{[2\pi(v_0^\infty)^2]^{3/2}} \exp\left(-\frac{|v|^2}{2(v_0^\infty)^2}\right) \quad [3]$$

where c_0^{ref} and v_0^∞ denote a reference concentration and the thermodynamic average speed, respectively. The reference concentration can be chosen from the ideal gas law as

$$c_0^{\text{ref}} = \frac{P_0}{R_g T} \quad [4]$$

where the partial pressure of species 0 is given by $P_0 = x_0 P_{\text{total}}$ based on the given mole fraction x_0, and R_g denotes the universal gas constant; see Table I. The temperature T in this paper is the constant and spatially uniform temperature in Table I. The thermal average speed, which is used in the Maxwellian, is given by

$$v_0^\infty = \sqrt{R_0 T} = \sqrt{\frac{k_B}{m_0} T} = \sqrt{\frac{R_g}{\omega_0} T} \quad [5]$$

based on the molecular weight ω_0. The universal gas constant R_g and the universal Boltzmann constant k_B are related through Avogadro's number N_A by $R_g = N_A k_B$; see Table I. Writing $(v_0^\infty)^2 = R_0 T$ results in another common representation of the Maxwellian

$$M_0^{\text{ref}}(v) = \frac{c_0^{\text{ref}}}{(2\pi R_0 T)^{3/2}} \exp\left(-\frac{|v|^2}{2R_0 T}\right) \quad [6]$$

Note that the Maxwellian is designed to have the same units as the density functions $f^{(i)}$.

Using the explicit solution for the background species, we solve the linear Boltzmann equation for the reactive species

Table I. Physical constants, operating conditions, and species reference quantities.

Physical constants	
Universal gas constant	$R_g = 8.3145$ J/(K mol) $= 62400$ (cm^3 Torr)/(K mol)
Universal Boltzmann constant	$k_B = 1.3807 \times 10^{-23}$ J/K
Avogadro's number	$N_A = 6.0221 \times 10^{23}$/mol
Operating conditions	
Ambient temperature	$T = 500$ K
Total pressure	$P_{\text{total}} = 1$ Torr
Reference quantities for inert background species I ($i = 0$)	
Mole fraction	$x_0 = 0.90$
Partial pressure	$P_0 = 0.90$ Torr
Reference concentration	$c_0^{\text{ref}} = 28.8 \times 10^{-9}$ mol/cm^3
Molecular weight	$\omega_0 = 4$ g/mol
Thermal average speed	$v_0^\infty = 10.0 \times 10^4$ cm/s
Reference quantities for reactive species A ($i = 1$)	
Mole fraction	$x_1 = 0.10$
Partial pressure	$P_1 = 0.10$ Torr
Reference concentration	$c_1^{\text{ref}} = 3.2 \times 10^{-9}$ mol/cm^3
Molecular weight	$\omega_1 = 104$ g/mol
Thermal average speed	$v_1^\infty = 2.0 \times 10^4$ cm/s

$$\frac{\partial f^{(1)}}{\partial t} + v\nabla_x f^{(1)} = Q_1(f^{(1)}) \quad [7]$$

with the linear collision operator $Q_1(f^{(1)}) := Q_{10}(f^{(1)}, M_0^{\text{ref}})$. Notice that decoupling from the background gas relied materially on the assumption that it is an inert gas.

Define a reference Maxwellian also for the reactive species by

$$M_1^{\text{ref}}(v) = \frac{c_1^{\text{ref}}}{[2\pi(v_1^\infty)^2]^{3/2}} \exp\left(-\frac{|v|^2}{2(v_1^\infty)^2}\right) \quad [8]$$

where c_1^{ref} and v_1^∞ denote again a reference concentration and the thermodynamic average speed for the species. They are chosen similarly as for the background species, see Table I.

The reference quantities for the nondimensionalization procedure are listed in Table II. The reference concentration c^* and reference speed v^* are chosen equal to the corresponding quantities for the reactive species. After defining the reference length appropriate for the domain size as $L^* = 1$ μm, we obtain on one hand the reference time for transport from $t^* = L^*/v^*$. The mean free path λ is about 100 μm at the operating conditions listed in Table I and de-

Table II. Reference quantities.

For gaseous species	
Reference concentration	$c^* := c_1^{\text{ref}} = 3.2 \times 10^{-9}$ mol/cm^3
Reference speed	$v^* := v_1^\infty = 2.0 \times 10^4$ cm/s
For transport	
Reference length	$L^* = 1$ μm $= 10^{-4}$ cm
Reference time for transport	$t^* = L^*/v^* = 5 \times 10^{-9}$ s $= 5$ ns
For collisions	
Mean free path	$\lambda = 100$ μm $= 10^{-2}$ cm
Reference time for collisions	$\tau^* = \lambda/v^* = 5 \times 10^{-7}$ s
For reactions	
(Formal) reference flux	$\eta^* := c^* v^* = 6.4 \times 10^{-5}$ mol/(s cm^2)
Total concentration of surface sites	$S_T = 10^{-9}$ mol/cm^2

Table III. Dimensionless variables.

Time	$\hat{t} = \frac{t}{t^*}$
Lengths	$\hat{x} = \frac{x}{L^*}$
Velocities	$\hat{v} = \frac{v}{v^*},\ \hat{v}_i^{\infty} = \frac{v_i^{\infty}}{v^*}$
Concentrations	$\hat{c}_i = \frac{c_i}{c^*},\ \hat{c}_i^{\mathrm{ref}} = \frac{c_i^{\mathrm{ref}}}{c^*}$
	$\hat{c}_i^{\mathrm{top}} = \frac{c_i^{\mathrm{top}}}{c^*},\ \hat{c}_i^{\mathrm{ini}} = \frac{c_i^{\mathrm{ini}}}{c^*}$
Density distributions	$\hat{f}^{(i)} = \frac{(v^*)^3}{c^*} f^{(i)}$
	$\hat{f}_i^{\mathrm{top}} = \frac{(v^*)^3}{c^*} f_i^{\mathrm{top}}$
	$\hat{f}_i^{\mathrm{ini}} = \frac{(v^*)^3}{c^*} f_i^{\mathrm{ini}}$
Maxwellians	$\hat{M}_i^{\mathrm{ref}} = \frac{(v^*)^3}{c^*} M_i^{\mathrm{ref}}$
Collision operators	$\hat{Q}_{ij} = \frac{(v^*)^3 \tau^*}{c^*} Q_{ij},$
	$\hat{Q}_i = \frac{(v^*)^3 \tau^*}{c^*} Q_i$
Fluxes, reaction rates	$\hat{\eta}_i = \frac{\eta_i}{\eta^*},\ \hat{R}_1 = \frac{R_1}{\eta^*}$
Fractional surface coverage	$\vartheta_A = \frac{S_A}{S_T}$

termines a reference time for collisions (the mean collision time) by $\tau^* = \lambda/v^*$. The ratio of those times or lengths is equal to the Knudsen number $\mathrm{Kn} = \lambda/L^* = \tau^*/t^*$.

The choices of dimensionless variables are listed in Table III. They result in the dimensionless Maxwellian

$$\hat{M}_1^{\mathrm{ref}}(\hat{v}) = \frac{\hat{c}_1^{\mathrm{ref}}}{[2\pi(\hat{v}_1^{\infty})^2]^{3/2}} \exp\left(-\frac{|\hat{v}|^2}{2(\hat{v}_1^{\infty})^2}\right) \quad [9]$$

where the dimensionless groups $\hat{c}_1^{\mathrm{ref}}$ and $\hat{v}_1^{\infty}$ are included in Table IV. The dimensionless Boltzmann equation is obtained by introducing the dimensionless variables in Table III. Notice that the left-hand side is nondimensionalized with respect to transport, while the right-hand side is nondimensionalized with respect to collisions. This results in the Knudsen number appearing in the dimensionless Boltzmann equation for the reactive species

$$\frac{\partial \hat{f}^{(1)}}{\partial \hat{t}} + \hat{v} \cdot \nabla_{\hat{x}} \hat{f}^{(1)} = \frac{1}{\mathrm{Kn}} \hat{Q}_1(\hat{f}^{(1)}) \quad [10]$$

Since Kn for gaseous flow on the feature scale is large, $\mathrm{Kn} \gg 1$ (see Table IV); we obtain the equation of free molecular flow

$$\frac{\partial \hat{f}^{(1)}}{\partial \hat{t}} + \hat{v} \cdot \nabla_{\hat{x}} \hat{f}^{(1)} = 0 \quad [11]$$

The surface reaction model.—We model the adsorption of molecules of A as reversible adsorption on a single site[13]

$$A + v \rightleftharpoons A_v \quad [12]$$

where A_v is adsorbed A, and v stands for a surface site available for adsorption. Although there are additional reaction steps for ALD and other practical processes, this adsorption/desorption reaction provides a good vehicle through which to demonstrate our transport and reaction modeling methodology, and it provides useful insight regarding modeling requirements.

Table IV. Dimensionless groups.

For species A ($i = 1$)	
Dimensionless reference concentration	$\hat{c}_1^{\mathrm{ref}} = 1.0$
Dimensionless reference speed	$\hat{v}_1^{\infty} = 1.0$
For transport and collisions	
Knudsen number	$\mathrm{Kn} := \lambda/L^* = 100$
For reactions	
Reaction coefficients for Reaction 1	$\gamma_1^f = S_T k_1^f,$
	$\gamma_1^b = \frac{S_T}{\eta^*} k_1^b$
Prefactor	$\alpha_p = \frac{\eta^* t^*}{S_T} = 0.32 \times 10^{-3}$

The total molar concentration of surface sites available for deposition is denoted by S_T, see Table II. If S_A denotes the concentration of adsorbed molecules of A, the difference $S_T - S_A$ is the concentration of vacant sites, and the reaction rate can be written as

$$R_1 = k_1^f(S_T - S_A)\eta_1 - k_1^b S_A \quad [13]$$

where η_1 denotes the flux of species to the surface, which is related to the distribution function of Eq. 1 by

$$\eta_1(x,t) = \int_{\nu \cdot v' > 0} |\nu \cdot v'| f^{(1)}(x,v',t) dv' \quad x \in \Gamma_w \quad [14]$$

Here, Γ_w denotes the points at the wafer surface and $\nu \equiv \nu(x)$ is the unit outward normal vector at $x \in \Gamma_w$. Notice that the integral is over all velocities pointing out of the domain due to the condition $\nu \cdot v' > 0$. The evolution of the concentration of sites occupied by A at every point x at the wafer surface Γ_w is given by

$$\frac{dS_A(x,t)}{dt} = R_1(x,t) \quad x \in \Gamma_w \quad [15]$$

Notice that this model assumes that there is no significant movement of molecules along the surface.

If we nondimensionalize the reaction rate with respect to the reference flux η^* and introduce the fractional surface coverage $\vartheta_A = S_A/S_T \in [0,1]$, we obtain the dimensionless reaction rate

$$\hat{R}_1 = \gamma_1^f(1 - \vartheta_A)\hat{\eta}_1 - \gamma_1^b \vartheta_A \quad [16]$$

with the dimensionless coefficients given in Table IV. Making the differential equation for S_A dimensionless, we obtain

$$\frac{d\vartheta_A(\hat{x},t)}{d\hat{t}} = \alpha_p \hat{R}_1(\hat{x},\hat{t}) \quad \hat{x} \in \Gamma_w \quad [17]$$

with the prefactor $\alpha_p = (\eta^* t^*)/S_T$. This differential equation is supplied with an initial condition that represents the fractional coverage $\vartheta_A^{\mathrm{ini}}$ at the initial time.

Note that it is in general impossible to find a closed-form solution $\vartheta_A(\hat{t})$ to the differential equation Eq. 17, because the coefficients involving $\hat{\eta}_1$ are not constant. But if this flux is constant, then Eq. 17 becomes a first-order linear ordinary differential equation with constant coefficients and can be solved analytically. Specifically, at each point on the feature surface, we have the problem

$$\frac{d\vartheta_A(\hat{t})}{d\hat{t}} = -\alpha_p b \vartheta_A(\hat{t}) + \alpha_p \gamma_1^f \hat{\eta}_1 \qquad \vartheta_A(0) = \vartheta_A^{\mathrm{ini}} \quad [18]$$

with $\alpha_p = (\eta^* t^*)/S_T$ and $b = \gamma_1^f \hat{\eta}_1 + \gamma_1^b$, which has the solution

$$\vartheta_A(\hat{t}) = \vartheta_A^{\infty}(1 - e^{-\alpha_p b \hat{t}}) + \vartheta_A^{ini} e^{-\alpha_p b \hat{t}} \quad [19]$$

with the equilibrium limit

$$\vartheta_A^{\infty} = \frac{\gamma_1^f \hat{\eta}_1}{\gamma_1^f \hat{\eta}_1 + \gamma_1^b} \quad [20]$$

provided that $\hat{\eta}_1$ is constant. Clearly, $\vartheta_A(\hat{t}) \to \vartheta_A^{\infty}$ as $\hat{t} \to \infty$, hence the name for the constant ϑ_A^{∞}. Note that this assumes that the species fluxes from the source above the wafer are constant. Equation 20 is also the solution of Eq. 16 with $\hat{R}_1$ set to zero (equilibrium).

Boundary conditions for the Boltzmann equation.—At the wafer surface, Γ_w, we use the boundary condition

$$f^{(1)}(x,v,t) = [\eta_1(x,t) - R_1(x,t)]C_1(x)M_1^{ref}(v) \quad \nu \cdot v < 0 \quad x \in \Gamma_w \quad [21]$$

where η_1 is the flux of species 1 to the surface and R_1 is the reaction rate of Reaction 1. The boundary condition assumes diffusive emission of molecules, *i.e.*, with the same velocity distribution as the reference Maxwellian.[10,12] In the absence of a reaction ($R_1 = 0$), the inflowing part of $f^{(1)}$ is then proportional to the flux to the surface η_1, because all molecules are being re-remitted. In the presence of a reaction though, the rate of reemission differs from the incoming flux by the reaction rate R_1, which could have either sign.

The factor C_1 is chosen as

$$C_1(x) = \left(\int_{\nu \cdot v<0} |\nu \cdot v| M_1^{ref}(v) dv \right)^{-1} \quad [22]$$

to guarantee mass conservation in the absence of reactions, that is, we require that influx equal to outflux for $R_1 = 0$

$$\int_{\nu \cdot v<0} |\nu \cdot v| f^{(1)}(x,v,t) dv = \int_{\nu \cdot v>0} |\nu \cdot v| f^{(1)}(x,v,t) dv \quad [23]$$

Notice that $C_1(x)$ depends on the position $x \in \Gamma_w$ via the unit outward normal vector $\nu(x)$.

Using the reference flux η^*, formally chosen as $\eta^* = c^* v^*$ (see Table II), the dimensionless boundary condition attains the same form as the dimensional one as

$$\hat{f}^{(1)}(\hat{x},\hat{v},\hat{t}) = [\hat{\eta}_1(\hat{x},\hat{t}) - \hat{R}_1(\hat{x},\hat{t})]\hat{C}_1(\hat{x})\hat{M}_1^{ref}(\hat{v}) \quad \nu \cdot \hat{v} < 0 \quad \hat{x} \in \Gamma_w \quad [24]$$

with the dimensionless flux to the surface

$$\hat{\eta}_1(\hat{x},\hat{t}) = \int_{\nu \cdot \hat{v}'>0} |\nu \cdot \hat{v}'| \hat{f}^{(1)}(\hat{x},\hat{v}',\hat{t}) d\hat{v}' \quad [25]$$

and with

$$\hat{C}_1(\hat{x}) = \left(\int_{\nu \cdot \hat{v}<0} |\nu \cdot \hat{v}| \hat{M}_1^{ref}(\hat{v}) d\hat{v} \right)^{-1} \quad [26]$$

The top of the domain of the feature scale model Γ_t forms the interface to the bulk of the gas domain in the reactor, and we assume that the distribution of $f^{(1)}$ is known there. More precisely, we assume that the inflow has a Maxwellian velocity distribution, hence

$$f^{(1)}(x,v,t) = f_1^{top} := \frac{c_1^{top}}{[2\pi(v_1^{\infty})^2]^{3/2}} \exp\left(-\frac{|v|^2}{2(v_1^{\infty})^2} \right) \quad \nu \cdot v < 0 \quad x \in \Gamma_t \quad [27]$$

Using the dimensionless variables in Table III results in the dimensionless boundary condition

$$\hat{f}^{(1)}(\hat{x},\hat{v},\hat{t}) = \hat{f}_1^{top} = \frac{\hat{c}_1^{top}}{[2\pi(\hat{v}_1^{\infty})^2]^{3/2}} \exp\left(-\frac{|\hat{v}|^2}{2(\hat{v}_1^{\infty})^2} \right) \quad \nu \cdot \hat{v} < 0 \quad \hat{x} \in \Gamma_t \quad [28]$$

On the sides of the domain Γ_s, which are perpendicular to the mean wafer surface, we use specular reflection for the boundary condition to simulate an infinite domain. This condition can immediately be stated in dimensionless form as

$$\hat{f}^{(1)}(\hat{x},\hat{v},\hat{t}) = \hat{f}^{(1)}(\hat{x},\hat{v}',\hat{t}) \quad \nu \cdot \hat{v} < 0 \quad \hat{x} \in \Gamma_s \quad [29]$$

with

$$\hat{v}' = \hat{v} - 2\nu(\nu \cdot \hat{v}) \quad [30]$$

Finally, we assume that the initial distribution of gas is given by

$$f^{(1)}(x,v,t) = f_1^{ini} := \frac{c_1^{ini}}{[2\pi(v_1^{\infty})^2]^{3/2}} \exp\left(-\frac{|v|^2}{2(v_1^{\infty})^2} \right) \quad x \in \Omega \quad t = 0 \quad [31]$$

with a Maxwellian velocity distribution; in particular, the choice of $c_1^{ini} = 0$ results in no gas of species 1 in the domain initially. The dimensionless initial condition is then

$$\hat{f}^{(1)}(\hat{x},\hat{v},\hat{t}) = \hat{f}_1^{ini} = \frac{\hat{c}_1^{ini}}{[2\pi(\hat{v}_1^{\infty})^2]^{3/2}} \exp\left(-\frac{|\hat{v}|^2}{2(\hat{v}_1^{\infty})^2} \right) \quad \hat{x} \in \Omega \quad \hat{t} = 0 \quad [32]$$

If the reference concentration in the reference Maxwellian is chosen as $c_1^{ref} = c_1^{top}$ and there are no surface reactions, the reference Maxwellian will be the exact equilibrium solution of the model by construction.

Numerical

This paper reports on numerical results obtained in two dimensions, and the numerics are stated in 2-D form here; the generalization to three dimensions is straightforward, but considerably more computationally intense. To simplify notation, the carets ($\hat{}$) used to indicate dimensionless variables are omitted in this section.

The solution $f^{(1)}(x,v,t)$ to the kinetic equation Eq. 11 together with the boundary conditions Eq. 24, 28, and 29, and the initial condition Eq. 32 depends on $x \in \Omega \subset \mathbb{R}^2$, $v \in \mathbb{R}^2$, and $t \geq 0$. Neglecting also the superscript of $f^{(1)}$ in this section to simplify notation, Eq. 11 for $f(x,v,t)$ in two dimensions reads explicitly

$$\frac{\partial f}{\partial t} + v^{(1)} \frac{\partial f}{\partial x_1} + v^{(2)} \frac{\partial f}{\partial x_2} = 0 \quad [33]$$

where $v^{(1)}$ and $v^{(2)}$ denote the components of the velocity vector $v = (v^{(1)}, v^{(2)}) \in \mathbb{R}^2$ in the x_1 and x_2 directions, respectively.

We approach the problem by discretizing the components of the velocity vector in Cartesian coordinates by $v_{k_1}^{(1)}$, $k_1 = 0, \ldots, K_1 - 1$, in the $v^{(1)}$ variable and by $v_{k_2}^{(2)}$, $k_2 = 0, \ldots, K_2 - 1$ in the

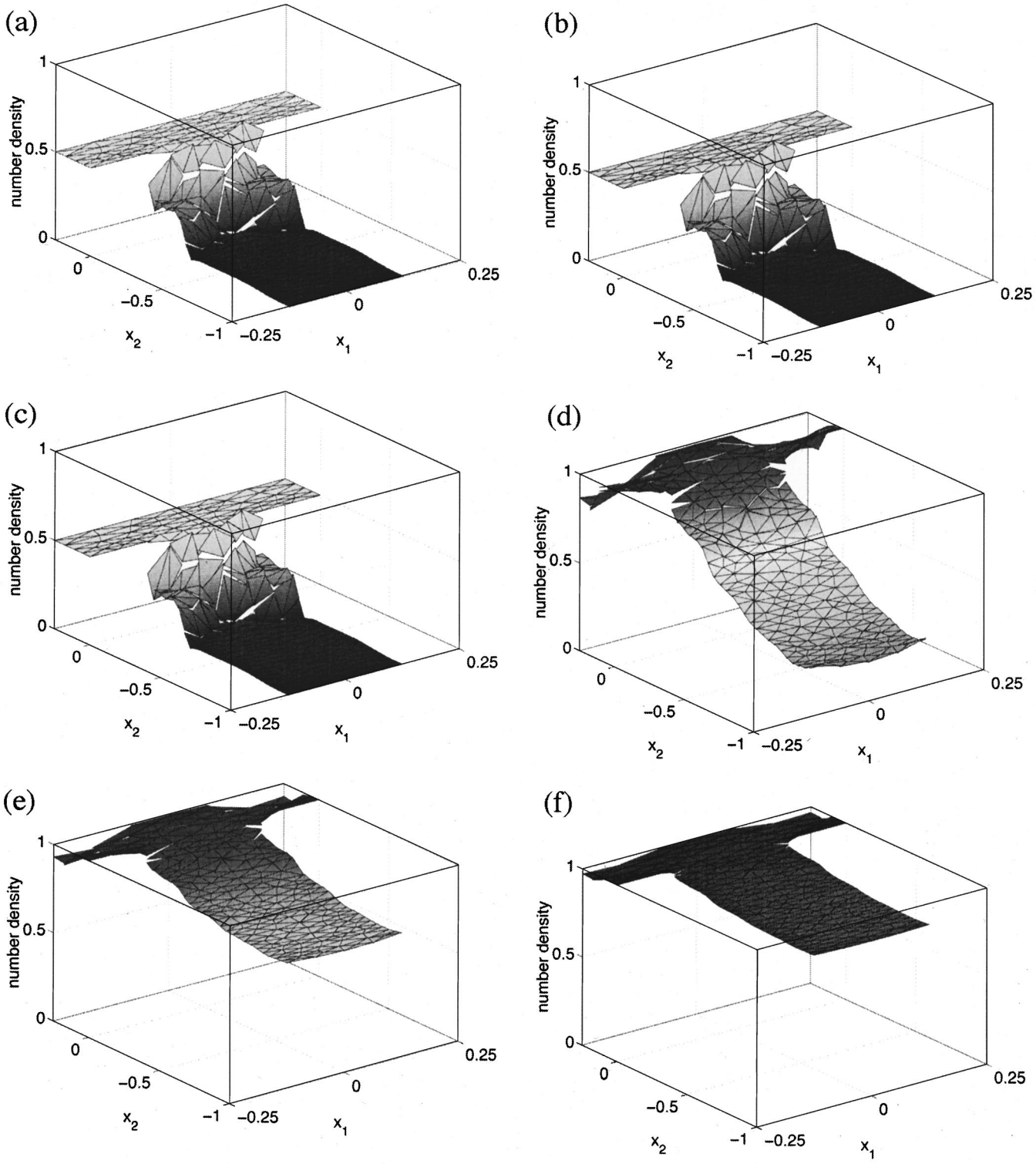

Figure 2. Adsorption step: dimensionless number density for a feature with aspect ratio $A = 4$ for $\gamma_1^f = 1.0$ and $\gamma_1^b = 0.01$ at times (a) 10.0 ns, (b) 40.0 ns, (c) 80.0 ns, (d) 1.0 ms, (e) 2.0 ms, (f) 3.0 ms. Note the different scales on the x_1 and the x_2 axes.

$v^{(2)}$ variable. The velocity discretization is then defined by $v_k = (v_{k_1}^{(1)}, v_{k_2}^{(2)})$, $k = 0, \ldots, K-1$, with $K = K_1K_2$, using the formulas $k_1 = k - K_1k_2$ and $k_2 = \lfloor k/K_1 \rfloor$.

Now expand the unknown f for the reactive species in velocity space

$$f(x,v,t) = \sum_{k=0}^{K-1} f_k(x,t)\varphi_k(v) \qquad [34]$$

where the $\varphi_k(v)$, $k = 0, 1, \ldots, K-1$, form an orthogonal set of

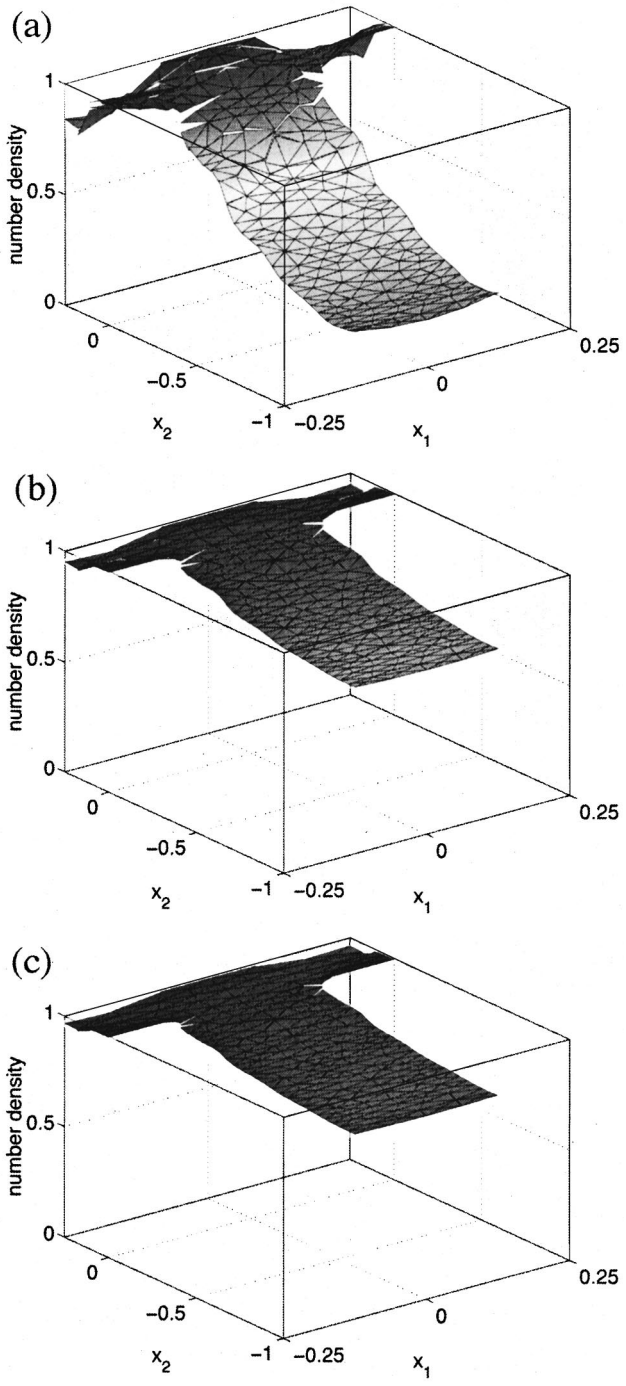

Figure 3. Adsorption step: dimensionless number density for a feature with aspect ratio $A = 4$ for $\gamma_1^f = 10^{-2}$ and $\gamma_1^b = 10^{-4}$ at times (a) 10.0 ns, (b) 40.0 ns, (c) 80.0 ns. Note the different scales on the x_1 and the x_2 axes.

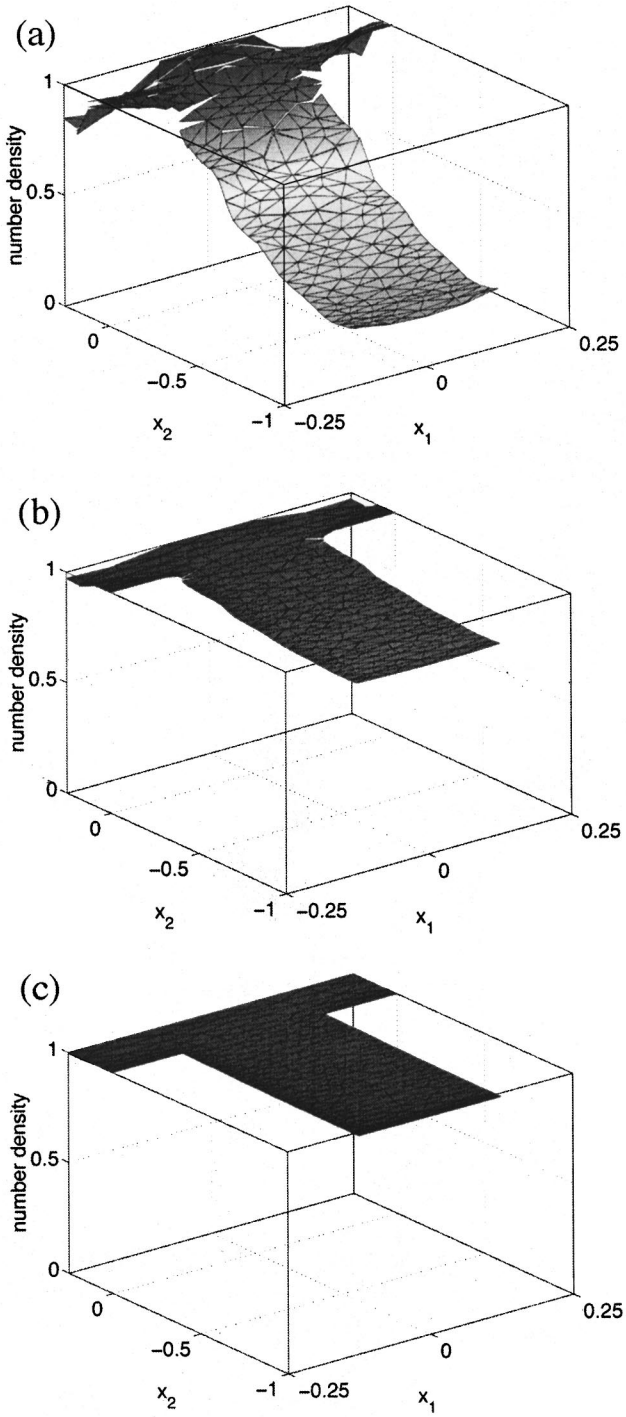

Figure 4. Adsorption step: dimensionless number density for a feature with aspect ratio $A = 4$ for $\gamma_1^f = 10^{-4}$ and $\gamma_1^b = 10^{-6}$ at times (a) 10.0 ns, (b) 40.0 ns, (c) 80.0 ns. Note the different scales on the x_1 and the x_2 axes.

basis functions in velocity space with respect to some inner product $\langle \cdot , \cdot \rangle_C$, namely, $\langle \varphi_k, \varphi_k \rangle_C = q_k \neq 0$ for all k and $\langle \varphi_l, \varphi_k \rangle_C = 0$ for all $l \neq k$. Following ideas in Ref. 14, it is possible to make a judicious choice of basis functions such that it also holds that $\langle v^{(1)} \varphi_k, \varphi_k \rangle_C = q_k v_{k_1}^{(1)}$ and $\langle v^{(2)} \varphi_k, \varphi_k \rangle_C = q_k v_{k_2}^{(2)}$ for all k as well as $\langle v^{(1)} \varphi_l, \varphi_k \rangle_C = 0$ and $\langle v^{(2)} \varphi_l, \varphi_k \rangle_C = 0$ for all $l \neq k$.

To obtain an equivalent system of equations for the vector of coefficient functions

$$F(x,t) = \begin{pmatrix} f_0(x,t) \\ \vdots \\ f_{K-1}(x,t) \end{pmatrix} \qquad [35]$$

the expansion $f(x,v,t) = \Sigma_{l=0}^{K-1} f_l(x,t) \varphi_l(v)$ from Eq. 34 is inserted into Eq. 33 and the resulting equation is tested against φ_k in the scalar product $\langle \cdot , \cdot \rangle_C$. This Galerkin approach yields

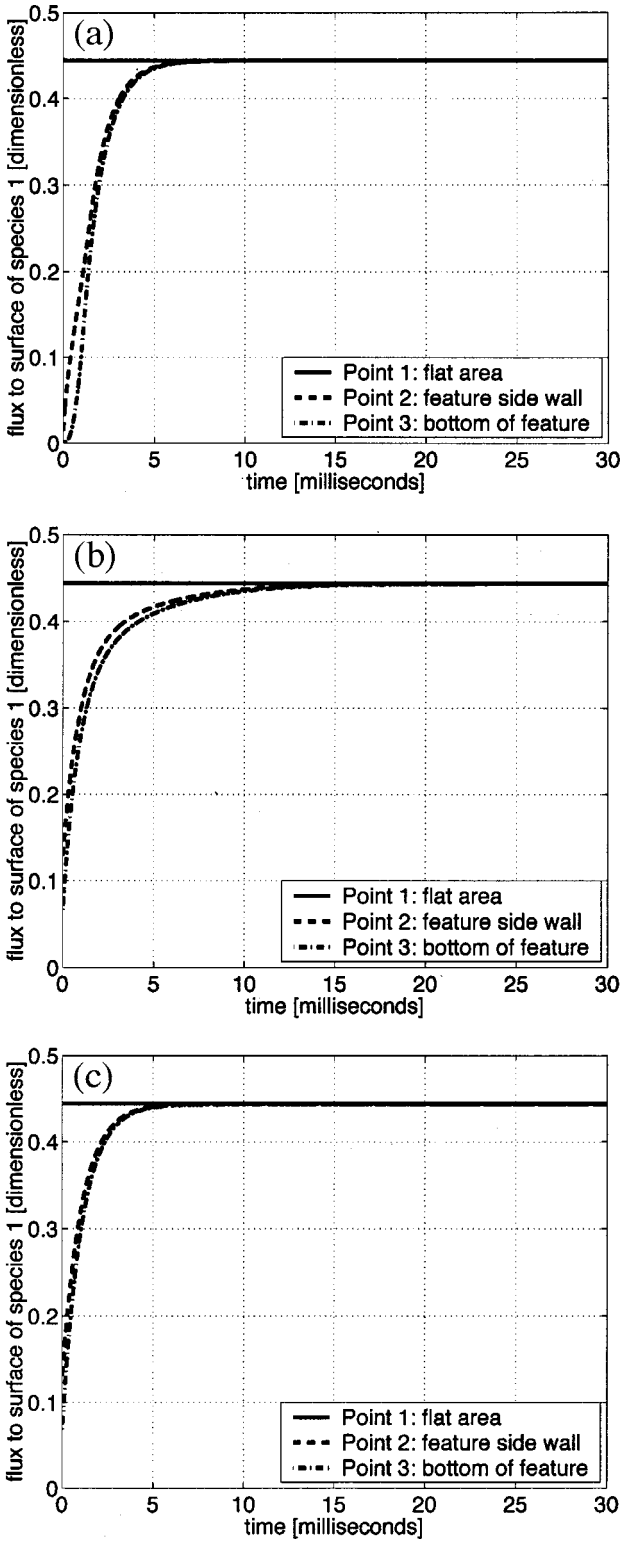

Figure 5. Adsorption step: dimensionless flux to the surface *vs.* time at the three observation points (see Fig. 1a) for $\gamma_1^b = \gamma_1^f/100$ with (a) $\gamma_1^f = 1.0$, (b) $\gamma_1^f = 10^{-2}$, (c) $\gamma_1^f = 10^{-4}$.

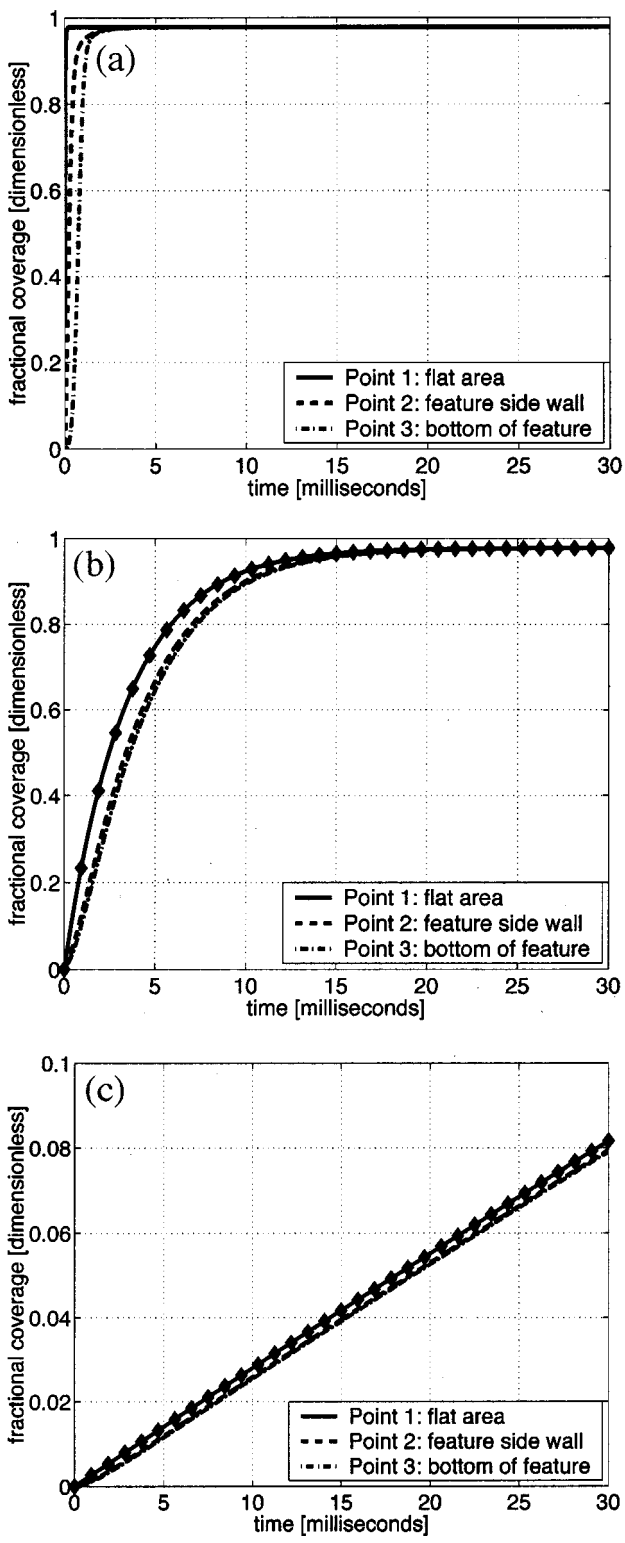

Figure 6. Adsorption step: fractional coverage *vs.* time at the three observation points (see Fig. 1a) for $\gamma_1^b = \gamma_1^f/100$ with (a) $\gamma_1^f = 1.0$, (b) $\gamma_1^f = 10^{-2}$, (c) $\gamma_1^f = 10^{-4}$. The solid diamonds in (b) and (c) show the analytical solution given by Eq. 19. Notice the different scales on the vertical axes.

$$\sum_{l=0}^{K-1} \langle \varphi_l, \varphi_k \rangle_C \frac{\partial f_l}{\partial t} + \sum_{l=0}^{K-1} \langle v^{(1)} \varphi_l, \varphi_k \rangle_C \frac{\partial f_l}{\partial x_1} + \sum_{l=0}^{K-1} \langle v^{(2)} \varphi_l, \varphi_k \rangle_C \frac{\partial f_l}{\partial x_2} = 0 \qquad [36]$$

Using the properties of the basis functions from above, this system of linear hyperbolic equations can be written in vector form as

$$\frac{\partial F}{\partial t} + A^{(1)} \frac{\partial F}{\partial x_1} + A^{(2)} \frac{\partial F}{\partial x_2} = 0 \qquad [37]$$

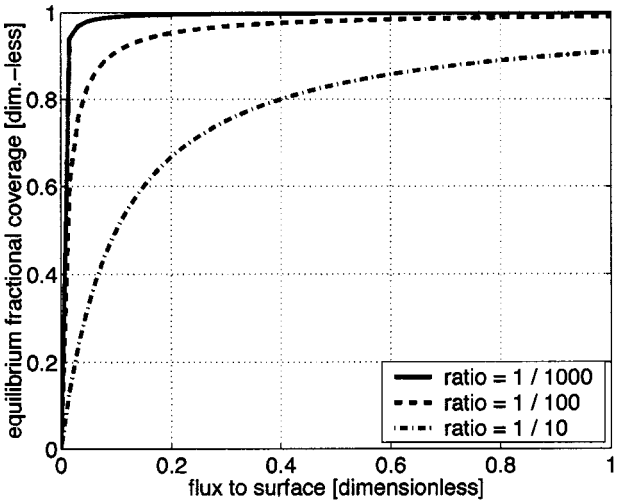

Figure 7. Langmuir isotherms according to analytical solution given by Eq. 19 for any value of γ_1^f and for various ratios of γ_1^b/γ_1^f.

with diagonal matrices $A^{(1)}$, $A^{(2)} \in \mathbb{R}^{K\times K}$ that have the entries $A^{(1)}_{kk} = v^{(1)}_{k_1}$ and $A^{(2)}_{kk} = v^{(2)}_{k_2}$. First mathematical results based on this approach can be found in Ref. 15, 16.

This system of linear hyperbolic equations is now posed in standard form amenable for numerical computations. However, due to its large size K, the irregular structure of the domain, and the requirement to compute for long times, it still poses a formidable challenge. It is solved using the discontinuous Galerkin method implemented in the code DG,[17] which is well-suited to the task. See Ref. 18, 19 for more detailed information on the numerical method.

The demonstration results presented in this paper are computed using four discrete velocities in each x_1 and x_2 direction; hence, there are $K = 16$ equations. Most results were checked against discretizations using six discrete velocities in each direction, and good agreement was found for each of these comparisons. The spatial domain was meshed coarsely to save on computation time. The mesh for the domain is shown in Fig. 1b. As shown below, the coarse mesh and the value of K are sufficient to show that the time scale for transport is much faster than the time scale for adsorption for reasonable adsorption chemistries. In turn, this leads to a significantly simpler model that has the analytical solution of Eq. 19 for the surface fractions.

Results

In this section, we report some simulation results for the adsorption step and the purge step that might be part of an ALD cycle. The model is given by the dimensionless equations presented in the previous section. Some parameter values used are listed in Table IV. In addition, we need to specify the (dimensionless) reaction parameters in Eq. 16; they are specified below. To complete the model, we need to choose the initial condition for the (dimensionless) gas concentration throughout the domain $\hat{c}_1^{ini}$ and for the fractional coverage ϑ_A^{ini}, as well as the coefficient in the boundary condition at the top of the domain $\hat{c}_1^{top}$; these values are different for the adsorption step and the purge step, and are specified in the following subsections.

In order to analyze the behavior of the flux $\hat{\eta}_1$ to the surface and of the fractional surface coverage ϑ_A over time, three points on the wafer surface are chosen as shown in Fig. 1a. Point 1 is located on the flat area of the wafer surface at $(-0.75L,0)$; during adsorption, we expect the fractional coverage to increase fastest at this point. Point 2 is located half-way down the trench and has x_2 coordinate $-0.5AL$; it initially sees less of the gas and take longer to reach full coverage. Point 3 is located at the bottom of the feature at $(-AL, 0)$; for features with large aspect ratios, it takes yet longer times for the gas to reach point 3. The fluxes $\hat{\eta}_1$ and the fractional coverages ϑ_A are shown as functions of time at these representative locations.

The adsorption step.—We assume for the adsorption step that no gas of species A is initially present in the domain by choosing $\hat{c}_1^{ini} = 0.0$, and that it is fed with a Maxwellian distribution at the top of the domain by choosing $\hat{c}_1^{top} = 1.0$. This is a spatially uniform step function along the boundary between the feature and the source (reactor) volume. Initially, there are no adsorbed molecules of A on the surface of the feature, hence, the fractional coverage is initially zero: $\vartheta_A^{ini} = 0.0$.

After running the simulator using a zero sticking factor ($\gamma_1^f = \gamma_1^b = 0.0$), to make sure that the solution was a uniform flux to each point on the surface, we selected several other values. To further validate the simulation method, and to gain insight into the basic behavior of the process, we consider the limiting adsorption coefficient of $\gamma_1^f = 1.0$. We also consider $\gamma_1^f = 10^{-2}$ and $\gamma_1^f = 10^{-4}$, as they seem more representative of surface chemistries likely to be used in ALD. For the simulations in this paper, we use $\gamma_1^b = \gamma_1^f/100$.

Figure 2 shows plots of computed (dimensionless) number density of species A computed using Eq. 2 as a function of position in the domain Ω at several (redimensionalized) points in time. Figure 2a plots $\hat{c}_1(x,t)$ at time $t = 10.0$ ns; it shows that the transport from the interface to the bulk of the gas phase to the flat wafer surface is very fast, as it essentially represents molecular speeds and short distances. Figures 2b and c show $\hat{c}_1$ at times $t = 40.0$ and 80.0 ns. Observe that the interior of the feature is not completely filled with gas at these times. The reason is that the gas gets consumed as a result of $\gamma_1^f = 1.0$, wherever it hits the wafer surface that has no adsorbate. Hence, these molecules do not reemit from the surface and reach the bottom of the feature. Figures 2d, e, and f show $\hat{c}_1$ at times $t = 1.0$, 2.0, and 3.0 ms, respectively. As these plots show, it takes about 3.0 ms for the feature to fill completely with gas.

Figure 3 shows $\hat{c}_1(x,t)$ for the value of $\gamma_1^f = 10^{-2}$ at times $t = 10.0$, 40.0, and 80.0 ns. Figure 3a again demonstrates that it takes less than 10.0 ns for gas to reach the flat parts of the wafer surface. However, for this more realistic value of the adsorption coefficient γ_1^f, comparably few gas molecules stick to the surface, and nearly all molecules get remitted from the boundary. Figure 3c demonstrates that it takes only on the order of 80.0 ns for the entire feature to be filled with gas.

Figure 4 shows the corresponding results for the adsorption coefficient $\gamma_1^f = 10^{-4}$. Comparing Fig. 3c and 4c, observe that the feature is filled slightly more rapidly than for $\gamma_1^f = 10^{-2}$. This is reasonable, as even fewer molecules adsorb on the feature surface than for the case of $\gamma_1^f = 10^{-2}$. So, for reasonable adsorption rates, features fill on the time scale of about 100 ns.

Figure 5 shows plots of the (dimensionless) flux $\hat{\eta}_1$ of species A to the surface *vs.* time for the three values of the adsorption coefficient γ_1^f. Figures 5a, b, and c show plots for $\gamma_1^f = 1.0$, 10^{-2}, and 10^{-4}, respectively. The fluxes to the surface at points 1, 2, and 3 tend to the same steady-state value of about $\hat{\eta}_1^\infty = 0.444$, independent of the value of γ_1^f; this precise value for $\hat{\eta}_1^\infty$ is taken from the data files, from which the plots in Fig. 5 are produced. This is the flux of species A to the wafer surface and through the feature mouth. Figures 5a, b, and c show that the initial behavior depends on the value of γ_1^f, in agreement with the corresponding Fig. 2, 3, and 4, respectively. Observe that the feature fills with gas and the flux tends to a constant, spatially uniform value on the time scale of a ten milliseconds.

Figures 6a, b, and c show plots of the (dimensionless) coverage ratio ϑ_A *vs.* time up to $t = 30.0$ ms for $\gamma_1^f = 1.0$, 10^{-2}, and 10^{-4}, respectively. Figure 6a shows that the fractional coverage ϑ_A

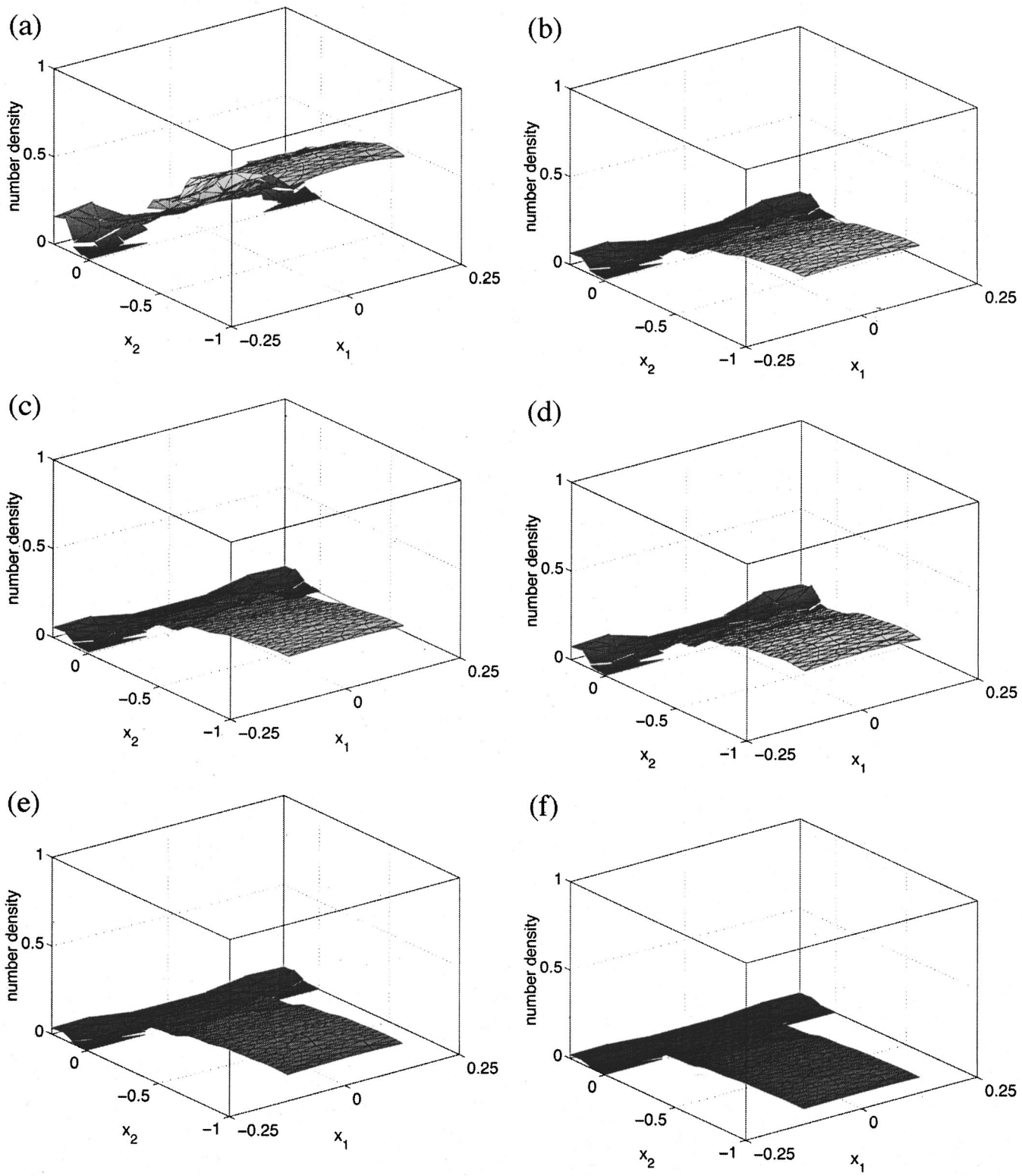

Figure 8. Purge step: dimensionless number density for a feature with aspect ratio $A = 4$ for $\gamma_1^f = 1.0$ and $\gamma_1^b = 0.01$ at times (a) 10.0 ns, (b) 40.0 ns, (c) 80.0 ns, (d) 1.0 ms, (e) 2.0 ms, (f) 3.0 ms. Note the different scales on the x_1 and the x_2 axes.

increases up to its equilibrium value relatively quickly for $\gamma_1^f = 1.0$. The time lags for points 2 and 3 are explained by the fact that it takes time for gas molecules to reach those areas inside the feature. Note that it takes about 3.0 ms to achieve coverage at all three points, which is another way to view the results shown in Fig. 2f. Figures 6b and c show that the fractional coverage increases more slowly for $\gamma_1^f = 10^{-2}$ and 10^{-4}, respectively. This is the case despite the fact that the feature is filled with gas much faster for these smaller values of γ_1^f. The development of the coverage ratio also indicates that the time to reach equilibrium coverage might be

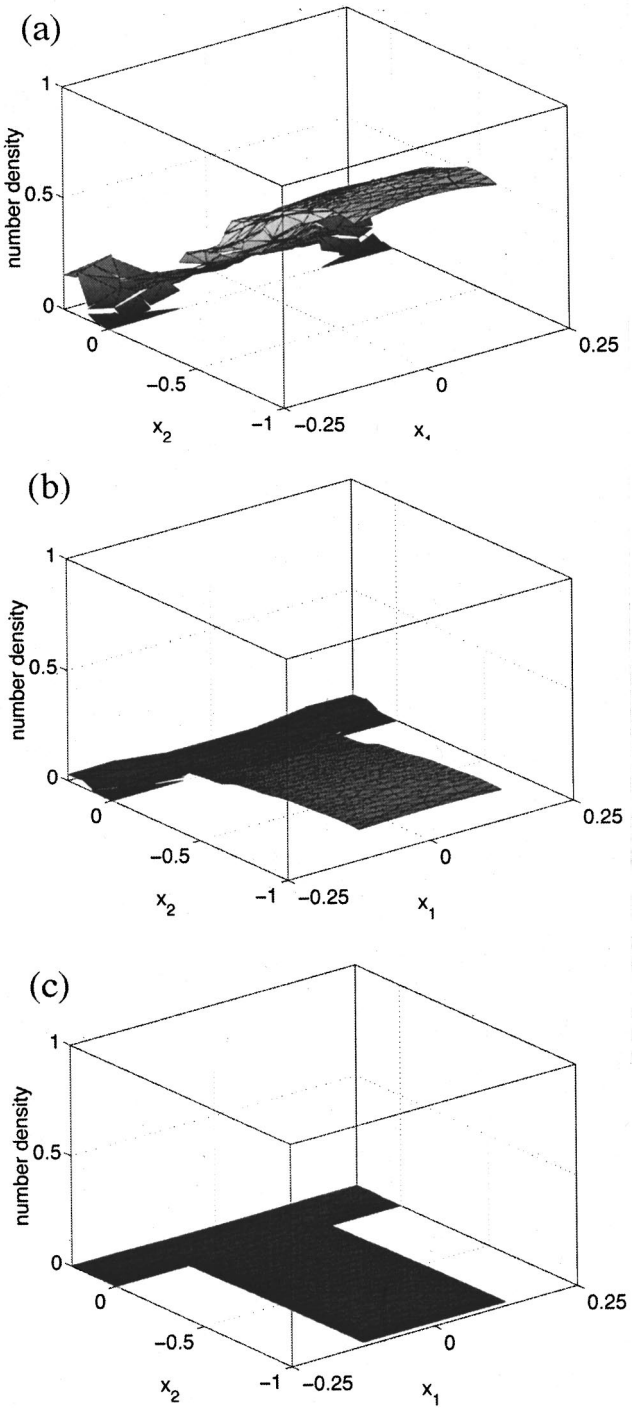

Figure 9. Purge step: dimensionless number density for a feature with aspect ratio $A = 4$ for $\gamma_1^f = 10^{-2}$ and $\gamma_1^b = 10^{-4}$ at times (a) 10.0 ns, (b) 40.0 ns, (c) 80.0 ns. Note the different scales on the x_1 and the x_2 axes.

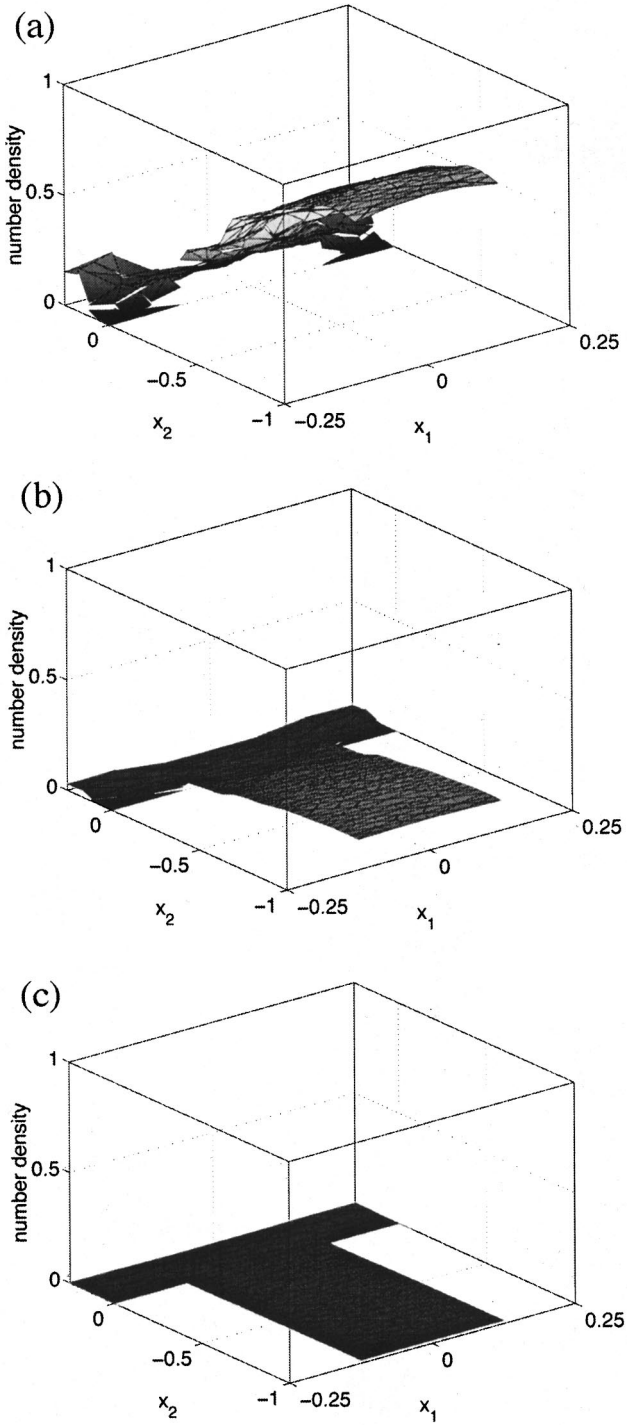

Figure 10. Purge step: dimensionless number density for a feature with aspect ratio $A = 4$ for $\gamma_1^f = 10^{-4}$ and $\gamma_1^b = 10^{-6}$ at times (a) 10.0 ns, (b) 40.0 ns, (c) 80.0 ns. Note the different scales on the x_1 and the x_2 axes.

inversely proportional to the value of γ_1^f, by comparing Fig. 6a and b; Fig. 6c shows ϑ_A still in its initial linear phase and cannot be used for this comparison.

The observations in Fig. 5 and 6 justify the approximation of $\hat{\eta}_1$ in Eq. 18 by the constant, spatially uniform flux $\hat{\eta}_1^\infty = 0.444$. Using this value in Eq. 19 with initial condition $\vartheta_A^{ini} = 0.0$, we are able to obtain an analytical representation of $\vartheta_A(\hat{t})$. This analytical prediction is incorporated into the Fig. 6b and c as the solid diamonds. Observe the good agreement with the simulation results.

We can estimate the equilibrium coverage from the analytical solution in Eq. 19 (or using Eq. 16 with $\hat{R}_1 = 0$) as

$$\vartheta_A(t) \to \vartheta_A^\infty = \frac{\gamma_1^f \hat{\eta}_1}{\gamma_1^f \hat{\eta}_1 + \gamma_1^b} = \frac{1}{1 + \dfrac{\gamma_1^b}{\gamma_1^f \hat{\eta}_1}} \quad \text{as} \quad \hat{t} \to \infty \quad [38]$$

Notice that the equilibrium value depends only on $\hat{\eta}_1$ at equilibrium and on the ratio γ_1^b/γ_1^f, but not on the value of γ_1^f itself. In this

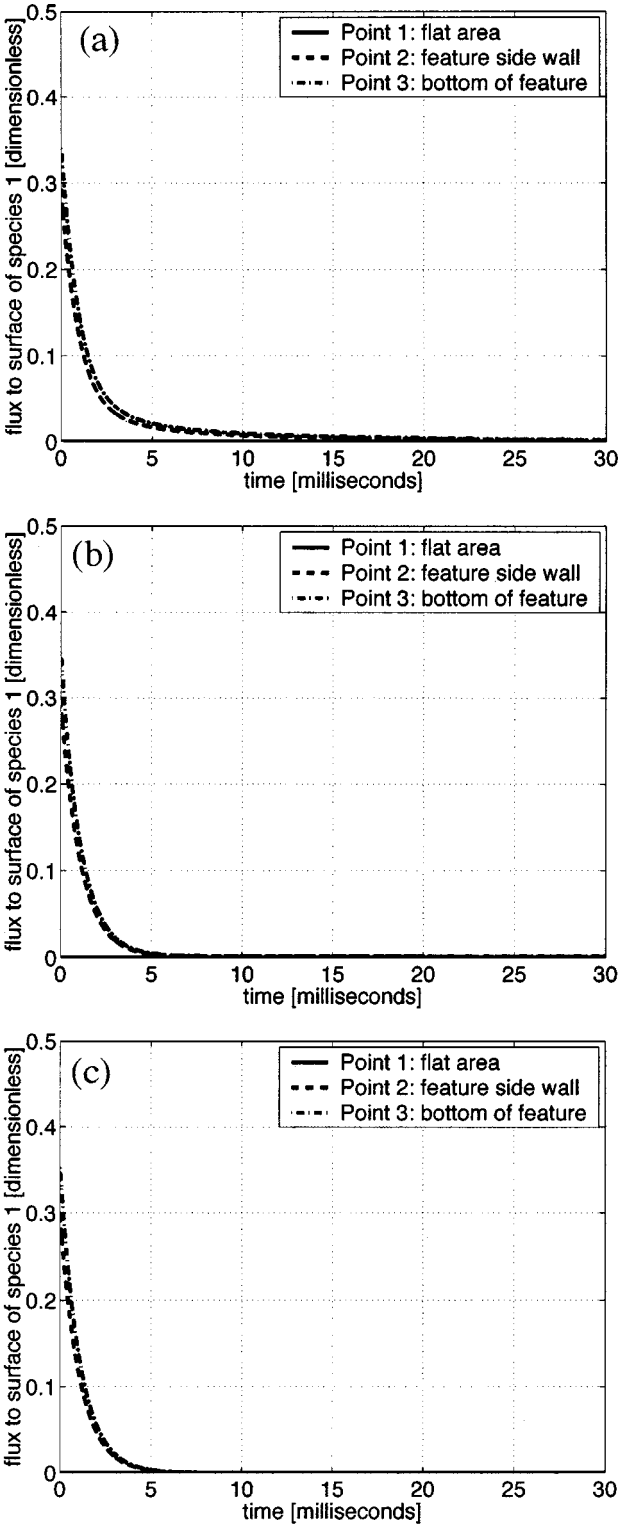

Figure 11. Purge step: dimensionless flux to the surface *vs.* time at the three observation points (see Fig. 1a) for $\gamma_1^b = \gamma_1^f/100$ with (a) $\gamma_1^f = 1.0$, (b) $\gamma_1^f = 10^{-2}$, (c) $\gamma_1^f = 10^{-4}$.

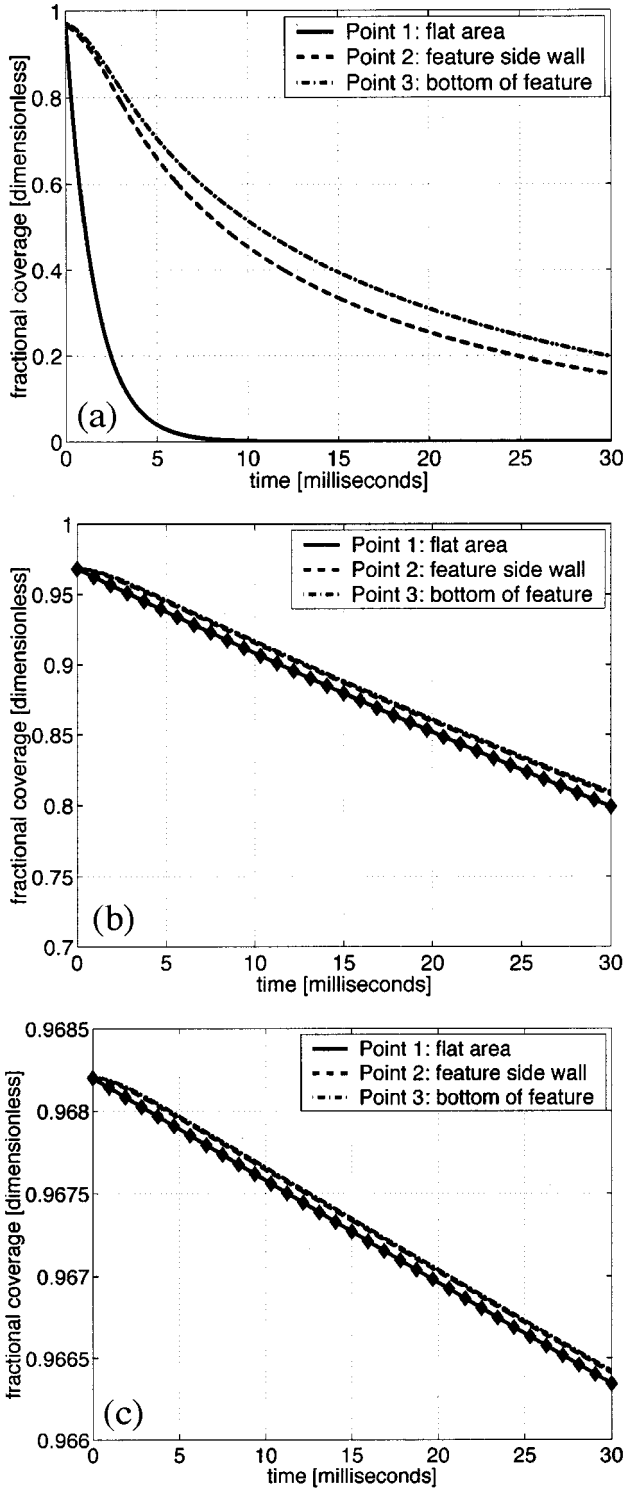

Figure 12. Purge step: fractional coverage *vs.* time at the three observation points (see Fig. 1a) for $\gamma_1^b = \gamma_1^f/100$ with (a) $\gamma_1^f = 1.0$, (b) $\gamma_1^f = 10^{-2}$, (c) $\gamma_1^f = 10^{-4}$. The solid diamonds in (b) and (c) show the analytical solution given by Eq. 19. Notice the different scales on the vertical axes.

study, $\hat{\eta}_1 \to 0.444$ and $\gamma_1^b/\gamma_1^f = 1/100$, and we calculate the value $\vartheta_A^\infty \approx 0.977974$, which is in excellent agreement with the observed values of 0.977975 and 0.977817 from the data used to generate Fig. 6a and b, respectively.

Also based on the analytical result, we can predict the time to reach 99% of equilibrium coverage by requiring that $\vartheta_A(\hat{t}_{0.99}) = 0.99\vartheta_A^\infty$ to find (in redimensionalized time)

$$t_{0.99} = -\ln(0.01)\,\frac{S_T}{\eta^*}\,\frac{1}{\gamma_1^f\hat{\eta}_1 + \gamma_1^b} \qquad [39]$$

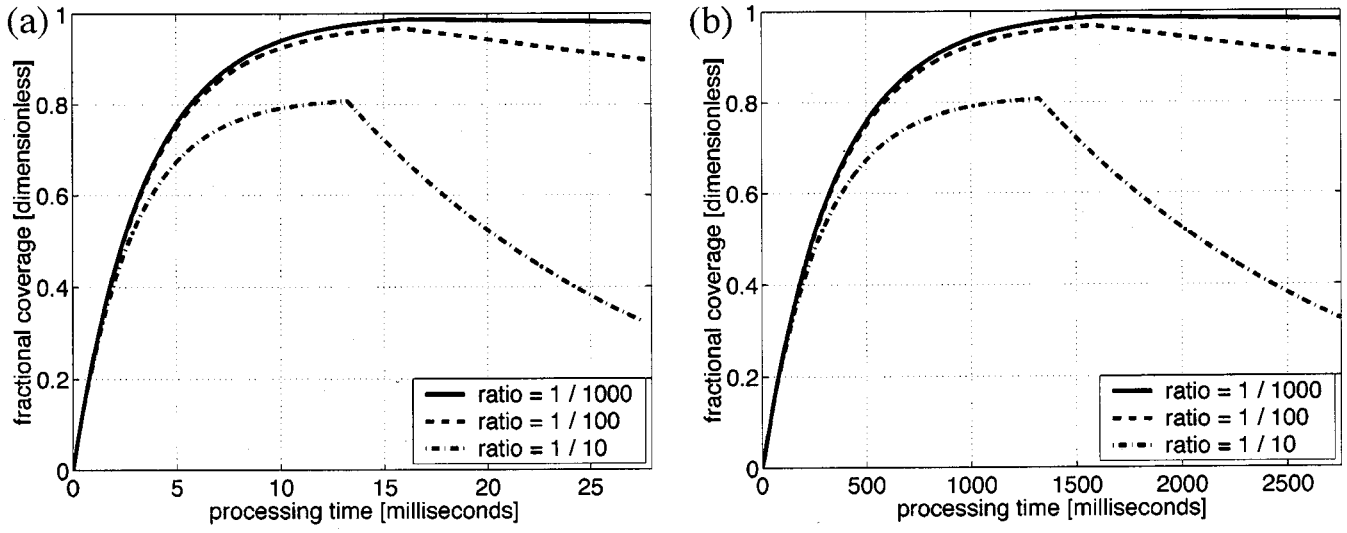

Figure 13. Fractional coverage *vs.* processing time for adsorption and purge together for various ratios of γ_1^b/γ_1^f with (a) $\gamma_1^f = 10^{-2}$, (b) $\gamma_1^f = 10^{-4}$. Processing time for adsorption is depicted up to 99% of equilibrium coverage.

provided that $\gamma_1^f \ll 1.0$. Using $\hat{\eta}_1 = 0.444$ and $\gamma_1^b = \gamma_1^f/100$, we find $t_{0.99} \approx 0.016$ s = 16.0 ms for $\gamma_1^f = 10^{-2}$. This time is in excellent agreement with the results shown in Fig. 6b. For $\gamma_1^f = 10^{-4}$, we obtain in the same way $t_{0.99} \approx 1.6$ s, which agrees with the observation that the time to reach equilibrium is inversely proportional to γ_1^f for $\gamma_1^f \ll 1.0$ and $\gamma_1^b \ll \gamma_1^f$.

To analyze the influence of the ratio γ_1^b/γ_1^f, Fig. 7 shows the (Langmuir) isotherms of the equilibrium coverage ϑ_A^∞ *vs.* the equilibrium flux $\hat{\eta}_1^\infty$ according to the analytical solution (or using Eq. 16 with $\hat{R}_1 = 0$) for any γ_1^f and for various ratios γ_1^b/γ_1^f. The plots indicate that equilibrium coverage depends strongly on the ratio of desorption rate parameter to adsorption rate parameter. It also depends on flux, particularly at low equilibrium coverages; at high coverages, the flux dependence decreases as the maximum surface coverage is approached.

The purge step.—At the beginning of the purge step after adsorption, the domain is filled uniformly with gaseous molecules, hence $\hat{c}_1^{ini} = 1.0$ is set. But no more gas is fed from the top, hence $\hat{c}_1^{top} = 0.0$. As the initial condition for the fractional coverage ϑ_A^{ini}, we assume that ϑ_A has reached 99% of its equilibrium value in the preceding adsorption step; *i.e.*, we choose as initial condition for the purge simulations the value $\vartheta_A^{ini} = (0.99)(0.977974) = 0.9682$. We assume this value to be spatially uniform for demonstration purposes. The desorption rate coefficient γ_1^b is again taken as a constant ratio relative to the adsorption rate coefficient as $\gamma_1^b = \gamma_1^f/100$ in these simulations.

The following results for the purge step are organized in the same way as those for the adsorption step in the previous subsection. Figures 8, 9, and 10 show the time evolution of the dimensionless concentration $\hat{c}_1$ for $\gamma_1^f = 1.0$, 10^{-2}, and 10^{-4}, respectively. In all cases, $\hat{c}_1$ decreases to zero over time, because it is not being fed into the domain. The only source is from desorption. Observe that the desorption from the wafer surface for the case of $\gamma_1^f = 1.0$ and $\gamma_1^b = 0.01$ is fast enough to explain the relatively slow decrease of $\hat{c}_1$ in Fig. 8, relative to the faster decreases of $\hat{c}_1$ shown in Fig. 9 and 10, virtually independent of the particular value of $\gamma_1^f \ll 1.0$.

Figure 11 shows the evolution of the dimensionless flux to the surface $\hat{\eta}_1$. The flux to the surface decreases to zero along with the concentration $\hat{c}_1$ in agreement with the figures for the concentrations. For small values of γ_1^b, the flux to the surface is essentially zero after 5 ms.

Figure 12 shows the evolution of the dimensionless fractional coverage ϑ_A *vs.* time up to $t = 30.0$ ms. As Fig. 12a shows, the coverage can decrease to zero within a matter of milliseconds for the highest value of the desorption rate coefficient considered. Figure 12b and c shows that the coverage will also decrease for the smaller values of $\gamma_1^b = 10^{-4}$ and 10^{-6}, but it will do so more slowly. In fact, the graphs do not extend to long enough time to show the approach of ϑ_A to zero. However, it is clear that ϑ_A decreases with time, hence, the purge time must be limited in order to prevent too much desorption.

From the observation that the flux decreases to almost zero quickly relative to desorption for small values of γ_1^b, it is again possible to use the analytical solution Eq. 19 to approximate the long-term behavior of ϑ_A. Therefore, with $\hat{\eta}_1 \approx 0.0$ and $\vartheta_A^{ini} = 0.9682$, plots of the analytical solution are incorporated in Fig. 12b and c, and agree very well with the simulation results.

To estimate the time to allow a decrease of the coverage ϑ_A to 90% of its initial coverage for the purge step, we require that $\vartheta_A(\hat{t}_{0.90}) = 0.90\vartheta_A^{ini} = (0.90)(0.9682) = 0.87138$ to find (in redimensionalized time)

$$t_{0.90} = -\ln(0.90)\,\frac{S_T}{\eta^*}\,\frac{1}{\gamma_1^b} \qquad [40]$$

For $\gamma_1^f = 10^{-2}$ and $\gamma_1^b = 10^{-4}$, this yields $t_{0.90} \approx 0.016$ s = 16.0 ms. This is in excellent agreement with Fig. 12b. The corresponding estimate for $\gamma_1^f = 10^{-4}$ and $\gamma_1^b = 10^{-6}$ is $t_{0.90} \approx 1.6$ s. Observe that the time $t_{0.90}$ depends only on the desorption coefficient γ_1^b, but not on the adsorption coefficient γ_1^f.

Figure 13 combines the analytical solutions for the adsorption and purge steps to give a picture of processing time. Here, the processing time for adsorption is depicted up to 99% of equilibrium coverage. Observe that the processing times depend strongly on γ_1^f, while the value of γ_1^b mostly affects the purge time. Note that the time to reach 99% of equilibrium during adsorption takes less time for $\gamma_1^b/\gamma_1^f = 1/10$, because there are more vacant sites available as equilibrium is approached; this is also reflected in Eq. 39, because γ_1^f is a significant fraction of the denominator in this case.

Conclusions

A model and numerical method are presented that are used to simulate the transient adsorption and desorption that would occur

during ALD over micrometer scale features during integrated circuit fabrication. The assumptions for the Boltzmann equation-based model are presented, and no adjustable parameters are used. A simple reversible Langmuir adsorption model is used; kinetic parameter values are chosen for demonstration purposes.

We consider the case in which the flux of reactive species from the source volume to the wafer surface is constant in time, either at zero or at some selected values; *i.e.*, we idealize transients at the reactor scale, to focus on modeling feature scale transients. More general boundary conditions at the interface between the wafer surface and the reactor volume are certainly possible.

We present results for transients in number density, flux, and surface coverage, and show that for reasonable surface kinetics, the time scale for transport ($\approx$100 ns) is much shorter than the time scale for adsorption and desorption (milliseconds to seconds). This has significant implications for integrated multiscale process simulation, as it allows the resolution in time to be of the same order as process transients. Thus, previous integrated multiscale process simulation efforts can be extended to model pattern scale effects during transients.[20-22] These transients can be intrinsic or programmed to optimize some process or product property.[8]

Acknowledgments

M.K.G. acknowledges support by the National Science Foundation under grant DMS-9805547. T.S.C. acknowledges support from MARCO, the Defense Advanced Research Projects Agency, and New York State Office of Science, Technology, and Academic Research through the Interconnect Focus Center. The authors also thank the International Erwin Schrödinger Institute for Theoretical Physics (Vienna, Austria) for the kind hospitality and support while writing this paper. We also acknowledge support of the Wittgenstein Award 2000 of P. Markowich, financed by the Austrian Research Fund. Finally, we are grateful to C. Ringhofer and J.-F. Remacle, without whose help this work would not have been possible.

Rensselaer Polytechnic Institute assisted in meeting the publication costs of this article.

References

1. M. Ritala and M. Leskela, *Nanotechnology*, **10**, 19 (1999).
2. M. Leskela and M. Ritala, *J. Phys. IV*, **5**, 937 (1995).
3. T. Suntola, *Thin Solid Films*, **216**, 84 (1992).
4. H. Simon and J. Aarik, *J. Phys. D*, **30**, 1725 (1997).
5. T. S. Cale, T. P. Merchant, L. J. Borucki, and A. H. Labun, *Thin Solid Films*, **365**, 152 (2000).
6. T. S. Cale and V. Mahadev, in *Thin Films*, Vol. 22, p. 175, Academic Press, New York (1996).
7. T. S. Cale, T. P. Merchant, and L. J. Borucki, in *Proceedings of the Advanced Metallization Conference in 1998*, Materials Research Society, p. 737 (1999).
8. T. S. Cale, D. F. Richards, and D. Yang, *J. Comput.-Aided Mater. Des.*, **6**, 283 (1999).
9. M. K. Gobbert and T. S. Cale, in *Fundamental Gas-Phase and Surface Chemistry of Vapor-Phase Deposition II*, M. T. Swihart, M. D. Allendorf, and M. Meyyappan, Editors, PV 2001-13, p. 316. The Electrochemical Society Proceedings Series, Pennington, NJ (2001).
10. C. Cercignani, *The Boltzmann Equation and Its Applications*, Springer-Verlag, New York (1988).
11. C. Cercignani, *Rarefied Gas Dynamics: From Basic Concepts to Actual Calculations*, Cambridge University Press, New York (2000).
12. G. N. Patterson, *Introduction to the Kinetic Theory of Gas Flows*, University of Toronto Press, Ontario, CN (1971).
13. R. I. Masel, *Principles of Adsorption and Reaction on Solid Surfaces*, Wiley Interscience, New York (1996).
14. C. Ringhofer, *Acta Numer.*, **6**, 485 (1997).
15. M. K. Gobbert and C. Ringhofer, in *IMA Volumes in Mathematics and Its Applications*, Springer-Verlag, New York, Accepted for publication.
16. M. K. Gobbert and C. Ringhofer, *Multiscale Modeling and Simulation*, Submitted.
17. J.-F. Remacle, J. Flaherty, and M. Shephard, *SIAM J. Sci. Comput. (USA)*, Accepted for publication.
18. *Discontinuous Galerkin Methods: Theory, Computation and Applications; Lecture Notes in Computational Science and Engineering*, B. Cockburn, G. E. Karniadakis, and C.-W. Shu, Editors, Vol. 11, Springer-Verlag, New York (2000).
19. M. K. Gobbert, J.-F. Remacle, and T. S. Cale, Unpublished work.
20. M. K. Gobbert, T. P. Merchant, L. J. Borucki, and T. S. Cale, *J. Electrochem. Soc.*, **144**, 3945 (1997).
21. T. P. Merchant, M. K. Gobbert, T. S. Cale, and L. J. Borucki, *Thin Solid Films*, **365**, 368 (2000).
22. T. S. Cale, M. O. Bloomfield, D. F. Richards, K. E. Jansen, J. A. Tichy, and M. K. Gobbert, in *IMA Volumes in Mathematics and Its Applications*, Springer-Verlag, New York, Accepted for publication.